Research Article

An analytical and numerical approach for the $(1+1)$-dimensional nonlinear Kolmogorov–Petrovskii–Piskunov equation

A. Chand and J. Mohapatra*,

Abstract

The main focus of this work is to develop and implement an efficient local discontinuous Galerkin scheme for acquiring the numerical solution of the $(1+1)$-dimensional nonlinear Kolmogorov–Petrovskii–Piskunov equation. The proposed framework employs a local discontinuous Galerkin discretization technique in the spatial direction and a higher-order total variation diminishing Runge–Kutta scheme in the temporal direction. The L_2 stability of the local discontinuous Galerkin method, which is ensured by carefully selecting the interface numerical fluxes, is discussed in detail.

*Corresponding author

Received 7 May 2024; revised 27 July 2024; accepted 29 September 2024

Abhilash Chand
Department of Mathematics, National Institute of Technology Rourkela, India. e-mail: abhilashchand@yahoo.com

Jugal Mohapatra
Department of Mathematics, National Institute of Technology Rourkela, India. e-mail: jugal@nitrkl.ac.in

The Kudryashov technique is also employed in this work to acquire the analytical traveling wave solution of the governing Kolmogorov–Petrovskii–Piskunov equation. Furthermore, the comparison between the obtained analytical and numerical solutions is demonstrated by computing the L_2 and L_∞ error norms. The accuracy and efficacy of the numerical local discontinuous Galerkin method solutions are validated by comparing them with analytical Kudryashov method solutions. For a more comprehensive understanding of the obtained analytical solutions, various graphical illustrations are presented in both two-dimensional and three-dimensional representations.

AMS subject classifications (2020): 35B35, 35G30, 65M60, 65N30.

Keywords: The Kolmogorov–Petrovskii–Piskunov equation; Kudryashov method; Local discontinuous Galerkin method; Total variation diminishing Runge–Kutta method; Stability analysis.

1 Introduction

Seeking analytical and numerical solutions for higher-order nonlinear evolution equations (NLEEs) has been an appealing and widely discussed topic for a long time. It has a significant impact on understanding the evolution of numerous nonlinear physical phenomena and is crucial when investigating nonlinear optics, coastal structures, plasma physics, biology, fluid physics, and other interrelated disciplines [3]. Over time, numerous researchers have developed a number of efficient and powerful methods for solving diverse nonlinear models, both analytically and numerically [25, 21, 1, 9]. Yan and Zhang [25] obtained new explicit solitary wave solutions of the WBK equation in shallow waters by a new generalized transformation based on the well-known Riccati equation. In their study, Santra and Mohapatra [21] employed a highly effective recursive numerical method to solve the multi-term time-fractional nonlinear KdV equation. Akkilic et al. [1] investigated the Jaulent-Miodek evolution equation using the $(m + 1/G')$-expansion and the rational sine-cosine methods. Ghosh and Mohapatra [9] utilized the Daftardar-Gejji and Jafari technique to address a fractional-order nonlinear diffusion model. In

the current work, we consider the $(1+1)$-dimensional nonlinear Kolmogorov–Petrovskii–Piskunov (KPP) equation, which is given in the following form:

$$u_t - u_{xx} + \mu u + \nu u^2 + \delta u^3 = 0, \quad (x,t) \in (a,b) \times (0,T] \tag{1}$$

with an initial condition

$$u(x,0) = u_0(x), \tag{2}$$

and boundary conditions

$$u(a,t) = \Psi_1(t) \text{and} u(b,t) = \Psi_2(t), \quad t \geq 0, \tag{3}$$

where μ, ν, and δ are arbitrary real parameters, and $u(x,t)$ represents the state evolution over the spatial-temporal domain specified by the x and t coordinates. The nonlinear KPP equation [19] which encompasses the Fisher, Newell–Whitehead, and Fitzhugh–Nagumo equation under certain conditions, is a mathematical model for studying many physical, chemical, and biological phenomena. When $\mu = -1$, $\nu = 1$, $\delta = 0$, the KPP (1) yields the Fisher equation [13]. When $\mu = -1$, $\nu = 0$, $\delta = 1$, the KPP (1) reduces to the Newell–Whitehead equation [12]. For $\nu = -(\mu+1)$, $\delta = 1$; the KPP (1) represents the Fitzhugh-Nagumo equation [20]. Over the years, many powerful analytical and numerical methods [8, 2, 14], have been implemented to solve the governing nonlinear KPP (1). Feng et al. [8] implemented the (G'/G)-expansion method in their study to acquire the traveling wave solutions of the nonlinear KPP (1). The Hermite collocation and SSPRK schemes are employed by Athanasakis, Papadopoulou, and Saridakis [2] to solve a generalized KPP equation numerically. Khater, Attia, and Lu [14] implemented the modified Khater method and B-spline schemes to solve a fractional model of the governing KPP (1).

This work implements the Kudryashov and the local discontinuous Galerkin (LDG) methods to acquire the analytical and numerical solutions for the nonlinear $(1+1)$-dimensional KPP equation. The analytical Kudryashov method was introduced and subsequently named after Kudryashov [15, 16] to construct exact traveling wave solutions for a wide range of nonlinear models. The Kudryashov method is based on implementation a special version of the

singularity manifold within the truncation procedure. This method enables us to reduce the challenge of acquiring exact solutions by solving the overdetermined system of algebraic equations. The key advantage of utilizing the Kudryashov technique is based on its remarkable ability to construct exact analytical solutions for higher-order NLEEs.

The LDG technique is one of the discontinuous Galerkin (DG) finite element methods that was initially proposed by Cockburn and Shu in a series of articles, which are listed in the review paper [23]. The LDG method is a highly appealing tool for solving a wide range of partial differential equations due to its versatility and success in handling mesh and shape functions. The LDG finite element approach is particularly noteworthy for its efficient handling of meshes with hanging nodes, elements of arbitrary structures, and variable local spaces. This feature enables effective hp-adaptivity, which leads to the interfacial layers and the complicated geometric structures of the solution being solved with high accuracy. The fundamental principle of the LDG technique, as outlined in this article, involves converting a given model with second-order derivatives into a system consisting only of first-order derivatives by employing auxiliary dependent variables. Following the discretization of the generated first-order system using the DG finite element spatial discretization scheme, a set of ordinary differential equations (ODEs) is produced. The ODEs are further discretized in time using the nonlinearly stable third-order total variation diminishing Runge–Kutta (TVD-RK3) methods [10] to obtain the desired numerical results. One notable advantage of the present LDG method framework is its provable L_2 stability, which is ensured by careful selection of the interface numerical fluxes that result from integration by parts. Chand and Saha Ray [5, 4] have successfully implemented the LDG technique to construct numerical solutions for the Allen–Cahn and Rosenau–Hyman equations. In addition, the LDG approach is used to examine various relevant equations in [24, 6, 7, 22, 11, 18].

This work represents the very first application of the numerical LDG scheme to the governing nonlinear KPP (1), thereby offering a novel contribution to the field. The present article is organized as follows: A comprehensive overview is presented in section 1. The analytical Kudryashov technique and its application in constructing an exact solution to the governing KPP (1)

are outlined in section 2. In section 3, the formulation and implementation of the LDG scheme algorithm, as well as spatial and TVD-RK3 temporal discretization techniques, are discussed in detail. The L_2 stability of the LDG method for governing KPP (1) is also established. Moreover, numerical simulations are included in section 4 to validate the accuracy and efficacy of the numerical LDG scheme in solving the nonlinear KPP (1). Finally, section 5 offers the conclusion of this work.

2 The Kudryashov method

This section presents the analytical solution of the governing KPP (1) using the Kudryashov technique. Consider the following traveling wave transformation by taking the combination of real variables x and t into a single variable ξ,

$$u(x,t) = U(\xi), \quad \xi = kx + ct, \tag{4}$$

where c and k are nonzero constants. The nonlinear KPP (1) is then reduced to the the following ODE for $u = U(\xi)$ using (4) as follows:

$$c\frac{\mathrm{d}U}{\mathrm{d}\xi} - k^2\frac{\mathrm{d}^2U}{\mathrm{d}\xi^2} + \mu U + \nu U^2 + \delta U^3 = 0. \tag{5}$$

2.1 Application of the Kudryashov method to the KPP equation

Let the solution $U(\xi)$ of ODE (5) be expressed as a finite expansion:

$$U(\xi) = \sum_{i=0}^{N} a_i \Phi^i(\xi), \quad \Phi(\xi) = \frac{1}{1 + \exp(\xi)}, \tag{6}$$

where $a_i(i = 0, \cdots, N, a_N \neq 0)$ denotes as-yet-undetermined constants and the positive integer N denotes the pole order for the general solution of (5). The function $\Phi(\xi)$ satisfies the first-order Riccati equation $\frac{\mathrm{d}\Phi}{\mathrm{d}\xi} = \Phi^2 - \Phi$.

Balancing U^3 and $\frac{\mathrm{d}^2 U}{\mathrm{d}\xi^2}$ in (5), it yields the pole for the general solution is of the first order, that is, $N = 1$. Hence, the analytical solution $U(\xi)$ of (5) has the following form:

$$U(\xi) = a_0 + a_1 \Phi, \quad a_1 \neq 0. \tag{7}$$

By plugging (7) and its derivatives into (5), it yields a polynomial in $\Phi(\xi)$ as follows:

$$\left(-2a_1 k^2 + a_1^3 \delta\right) \Phi^3 + \left(a_1 c + 3a_1 k^2 + 3a_0 a_1^2 \delta + a_1^2 \nu\right) \Phi^2$$
$$+ \left(-a_1 c - a_1 k^2 + 3a_0^2 a_1 \delta + a_1 \mu + 2a_0 a_1 \nu\right) \Phi + \left(a_0^3 \delta + a_0 \mu + a_0^2 \nu\right). \tag{8}$$

Now, equating the coefficients of $\Phi^i (i = 0, 1, \ldots, 3)$ to zero in (8) yields the set of simultaneous algebraic equations as follows:

$$\begin{aligned}
&\Phi^0 : a_0^3 \delta + a_0 \mu + a_0^2 \nu, \\
&\Phi^1 : -a_1 c - a_1 k^2 + 3a_0^2 a_1 \delta + a_1 \mu + 2a_0 a_1 \nu, \\
&\Phi^2 : a_1 c + 3a_1 k^2 + 3a_0 a_1^2 \delta + a_1^2 \nu, \\
&\Phi^3 : -2a_1 k^2 + a_1^3 \delta.
\end{aligned} \tag{9}$$

The family of nontrivial solutions of the set of algebraic equations (9) is as follows:

$$a_0 = \frac{-\nu - \sqrt{\Omega}}{2\delta}, \quad a_1 = \frac{9\mu\sqrt{\Omega} - \frac{2\nu^2 \sqrt{\Omega}}{\delta}}{9\delta\mu - 2\nu^2}, \quad c = \frac{\nu\sqrt{\Omega}}{2\delta}, \quad k = -\sqrt{\frac{\Omega}{2\delta}}, \tag{10}$$

where $\Omega = \nu^2 - 4\delta\mu$. So, by plugging (10) into expression (7) and simplifying the resulting equation, the analytical traveling wave solution of the governing KPP (1) is obtained as

$$\begin{cases}
u(x, t) = \dfrac{1}{2\delta} \left(-\nu + \sqrt{\Omega} \tanh\left(\dfrac{(\sqrt{2}x\sqrt{\delta} - t\nu)\sqrt{\Omega}}{4\delta}\right)\right), \\
\Omega = \nu^2 - 4\delta\mu,
\end{cases} \tag{11}$$

where μ, ν, and δ are arbitrary constants.

3 Numerical simulations for the KPP equation

An in-depth analysis of the LDG method for the governing KPP (1), including its algorithm development and practical implementation, is detailed in this section.

3.1 The LDG method for the KPP equation

Let the computational spatial domain $I = [a, b]$ be uniformly partitioned into the $\mathcal{M}$ nonoverlapping regular cells $I_m = \left[x_{m-\frac{1}{2}}, x_{m+\frac{1}{2}} \right]$, for $m = 1, \ldots, \mathcal{M}$, as follows:

$$a = x_{\frac{1}{2}} < x_{\frac{3}{2}} < \cdots < x_{\mathcal{M}+\frac{1}{2}} = b.$$

The cell center of I_m is $x_m = \frac{1}{2} \left(x_{m-\frac{1}{2}} + x_{m+\frac{1}{2}} \right)$, and the local mesh spacing is defined by $\delta x_m = \left(x_{m+\frac{1}{2}} - x_{m-\frac{1}{2}} \right)$, with maximal mesh being $\delta x = \max\limits_{m} \delta x_m$. Here, regular meshes signify that during the mesh refinement process, the mesh size ratio remains bounded. For formulating the LDG method algorithm, consider the solution and the test function space $V_{\delta x}^k$ to be defined as the following discontinuous finite element space:

$$V_{\delta x}^k = \{ v_m^l(x) : v_m^l(x) \in \mathcal{P}^k(I_m), \text{ for } x \in I_m, \ 1 \leqslant m \leqslant \mathcal{M}; \ 0 \leqslant l \leqslant k \}, \quad (12)$$

where $\mathcal{P}^k(I_m)$ represents the set of all polynomials with degrees no more than $k(\geq 0)$, on each cell I_m. Here, the piecewise scaled Legendre polynomials $\{ v_m^l(x), l = 0, 1, \ldots, k \}$, are used as the basis functions for the discontinuous solution space $V_{\delta x}^k$.

The numerical solution of the governing nonlinear KPP (1) is represented by u_h, with $u_h \in V_{\delta x}^k$ and is defined as follows:

$$u_h(x, t) = \sum_{l=0}^{k} u_m^l(t) v_m^l(x) = V^T(x) U_h(t), \text{ for } x \in I_m, \quad (13)$$

where $V(x) = (v_m^0, v_m^1, \ldots, v_m^k)^T$ and $U_h(t)$ denotes the degree of freedom across cell I_m. The $u_{m+1/2}^{\pm} = u_h(x_{m+1/2}^{\pm}, t)$ represents the right and left limits of u_h at the element boundary $x_{m+1/2}$.

3.2 Spatial discretization

To construct the LDG scheme algorithm, first, the governing $(1 + 1)$-dimensional KPP (1) that contains higher-order derivatives is transformed as a first-order system, and then DG finite element space discretization is implemented. So, by considering the auxiliary variable $r = u_x$, the governing nonlinear KPP (1) can be written as the following first-order system as follows:

$$\begin{cases} u_t - r_x = f(u), \\ r - u_x = 0, \end{cases} \tag{14}$$

where $f(u) = -(\mu u + \nu u^2 + \delta u^3)$ denotes the flux term. Now, the semi-discrete LDG scheme for the governing KPP (1) is defined as follows: To find a solution of (14) in terms of piecewise polynomial functions $u, r \in V_{\delta x}^k$, which satisfies (14) in a weak sense. So, we multiply (14) with test functions $w, z \in V_{\delta x}^k$ and integrate by parts over each cell I_m to obtain

$$\int_{I_m} u_t w \, dx + \int_{I_m} r w_x \, dx - (\widehat{r})_{m+\frac{1}{2}} (w)_{m+\frac{1}{2}}^- + (\widehat{r})_{m-\frac{1}{2}} (w)_{m-\frac{1}{2}}^+$$
$$= \int_{I_m} f(u) w \, dx, \tag{15}$$

$$\int_{I_m} r z \, dx + \int_{I_m} u z_x \, dx - (\widehat{u})_{m+\frac{1}{2}} (z)_{m+\frac{1}{2}}^- + (\widehat{u})_{m-\frac{1}{2}} (z)_{m-\frac{1}{2}}^+ = 0, \tag{16}$$

for all $m = 1, \ldots, \mathcal{M}$. The "hat" terms in (15) and (16) denote yet-to-be-determined "numerical fluxes", which are single-valued monotone functions defined on the element boundary $x_{m\pm\frac{1}{2}}$. The numerical fluxes are specifically designed to stabilize the LDG method and ensure the local solvability of auxiliary variables. Here, the following diffusion alternating fluxes [17], $\widehat{u}$ and $\widehat{r}$, are taken from opposite sides of the interface to ensure provable L_2 stability.

$$\widehat{u} = u^-, \quad \widehat{r} = r^+. \tag{17}$$

It is worth noting that the choice of numerical fluxes, as outlined in (17), need not be unique. The important step is to select $\widehat{u}$ and $\widehat{r}$ from the opposing sides. In this study, the boundary fluxes are chosen as follows:

$$\begin{cases} \widehat{u}_{\frac{1}{2}} = u(a,t), & \widehat{r}_{\frac{1}{2}} = r^+_{\frac{1}{2}}, \\ \widehat{u}_{\mathcal{M}+\frac{1}{2}} = u(b,t), & \widehat{r}_{\mathcal{M}+\frac{1}{2}} = r^-_{\mathcal{M}+\frac{1}{2}}. \end{cases} \tag{18}$$

This method is commonly referred to as a "local" DG method since it allows for the local elimination of the introduced auxiliary variables that approximate the derivatives of the solution. The detailed framework of the LDG scheme algorithm is now complete.

3.3 The TVD-RK3 temporal discretization

After DG finite element space discretization, the governing nonlinear KPP (1) yields the following ODE system of freedoms $\mathbf{U}$:

$$\frac{\mathrm{d}}{\mathrm{d}t}\mathbf{U} = L(\mathbf{U},t), \tag{19}$$

where $\mathbf{U} = (U_1, U_2, \ldots, U_{\mathcal{M}})^T$. The right-hand side of (19) is derived by eliminating the auxiliary variable r from (16). In the present work, the semi-discrete system (19) is time-integrated by utilizing the explicit TVD-RK3 time-stepping scheme [10], as follows:

$$\begin{cases} \mathbf{U}^{(1)} = \mathbf{U}^n + \delta t\, L(\mathbf{U}^n, t^n), \\ \mathbf{U}^{(2)} = \dfrac{3}{4}\mathbf{U}^n + \dfrac{1}{4}\mathbf{U}^{(1)} + \dfrac{1}{4}\delta t\, L(\mathbf{U}^{(1)}, t^n + \delta t), \\ \mathbf{U}^{n+1} = \dfrac{1}{3}\mathbf{U}^n + \dfrac{2}{3}\mathbf{U}^{(2)} + \dfrac{2}{3}\delta t\, L(\mathbf{U}^{(2)}, t^n + \dfrac{1}{2}\delta t), \end{cases} \tag{20}$$

where δt denotes the appropriate time step value.

3.4 Stability analysis

The L_2 stability property of the LDG method for nonlinear KPP (1) is discussed in this subsection. This is similar to the stability results in [24] for the time-dependent bi-harmonic type equation involving fourth derivatives.

Proposition 1 (L_2 stability)**.** The solution to the scheme (15) and (16) with the choice of numerical fluxes (17) is L_2 stable, that is,

$$\int_I \Big(\frac{1}{2} \frac{\mathrm{d}}{\mathrm{d}t} u^2(x,t) + r^2(x,t) \Big) \, \mathrm{d}x = \int_I f(u(x,t)) u(x,t) \, \mathrm{d}x. \tag{21}$$

Proof. First, summing up the two equalities in (15) and (16), we introduce the notation

$$\mathcal{B}_m(u,r;w,z) = \int_{I_m} u_t w \, \mathrm{d}x + \int_{I_m} r w_x \, \mathrm{d}x - (\widehat{r})_{m+\frac{1}{2}} (w)^-_{m+\frac{1}{2}}$$

$$+ (\widehat{r})_{m-\frac{1}{2}} (w)^+_{m-\frac{1}{2}} - \int_{I_m} f(u) w \, \mathrm{d}x + \int_{I_m} r z \, \mathrm{d}x + \int_{I_m} u z_x \, \mathrm{d}x$$

$$- (\widehat{u})_{m+\frac{1}{2}} (z)^-_{m+\frac{1}{2}} + (\widehat{u})_{m-\frac{1}{2}} (z)^+_{m-\frac{1}{2}}. \tag{22}$$

Since the solutions u, r of the scheme (15)–(17) clearly satisfy

$$\mathcal{B}_m(u,r;w,z) = 0, \tag{23}$$

for all test functions $w, z \in V^k_{\delta x}$, we can choose

$$w = u, \quad z = r.$$

With the above choices of test functions, (23) yields

$$\mathcal{B}_m(u,r;u,r) = \int_{I_m} u_t u \, \mathrm{d}x + \int_{I_m} r u_x \, \mathrm{d}x - (\widehat{r})_{m+\frac{1}{2}} (u)^-_{m+\frac{1}{2}}$$

$$+ (\widehat{r})_{m-\frac{1}{2}} (u)^+_{m-\frac{1}{2}} - \int_{I_m} f(u) u \, \mathrm{d}x + \int_{I_m} r^2 \, \mathrm{d}x + \int_{I_m} u r_x \, \mathrm{d}x$$

$$- (\widehat{u})_{m+\frac{1}{2}} (r)^-_{m+\frac{1}{2}} + (\widehat{u})_{m-\frac{1}{2}} (r)^+_{m-\frac{1}{2}} = 0. \tag{24}$$

Now, after simplification, we obtain

$$\frac{1}{2} \frac{\mathrm{d}}{\mathrm{d}t} \int_{I_m} u^2 \, \mathrm{d}x + \int_{I_m} r^2 \, \mathrm{d}x + \int_{I_m} (ur)_x \, \mathrm{d}x - \big(\widehat{r} u^- + \widehat{u} r^- \big)_{m+\frac{1}{2}}$$

$$+ \left(\widehat{r}u^+ + \widehat{u}r^+ \right)_{m-\frac{1}{2}} = \int_{I_m} f(u)u \, \mathrm{d}x. \qquad (25)$$

Next, using the definition (17) of the numerical fluxes and by summing up the equality (25) over all m, we obtain, after some algebraic manipulations,

$$\frac{1}{2} \frac{\mathrm{d}}{\mathrm{d}t} \int_I u^2 \, \mathrm{d}x + \int_I r^2 \, \mathrm{d}x$$

$$+ \sum_{m=1}^{\mathcal{M}} \left[(r)^+_{m-\frac{1}{2}} (u)^+_{m-\frac{1}{2}} - (r)^+_{m+\frac{1}{2}} (u)^-_{m+\frac{1}{2}} \right]$$

$$- \sum_{m=1}^{\mathcal{M}} \left[(u)^-_{m+\frac{1}{2}} (r)^-_{m+\frac{1}{2}} - (u)^-_{m-\frac{1}{2}} (r)^+_{m-\frac{1}{2}} \right]$$

$$+ \sum_{m=1}^{\mathcal{M}} \left[(u)^-_{m+\frac{1}{2}} (r)^-_{m+\frac{1}{2}} - (u)^+_{m-\frac{1}{2}} (r)^+_{m-\frac{1}{2}} \right] = \int_I f(u)u \, \mathrm{d}x.$$

This implies,

$$\frac{1}{2} \frac{\mathrm{d}}{\mathrm{d}t} \int_I u^2 \, \mathrm{d}x + \int_I r^2 \, \mathrm{d}x + \sum_{m=1}^{\mathcal{M}} \left[(u)^-_{m-\frac{1}{2}} (r)^+_{m-\frac{1}{2}} - (u)^-_{m+\frac{1}{2}} (r)^+_{m+\frac{1}{2}} \right]$$

$$= \int_I f(u)u \, \mathrm{d}x. \qquad (26)$$

Assuming the boundary conditions are either periodic or compactly supported, we easily obtain

$$\sum_{m=1}^{\mathcal{M}} \left[(u)^-_{m-\frac{1}{2}} (r)^+_{m-\frac{1}{2}} - (u)^-_{m+\frac{1}{2}} (r)^+_{m+\frac{1}{2}} \right] = 0,$$

and hence

$$\int_I \left(\frac{1}{2} \frac{\mathrm{d}}{\mathrm{d}t} u^2(x,t) + r^2(x,t) \right) \mathrm{d}x = \int_I f(u(x,t))u(x,t) \, \mathrm{d}x.$$

$\square$

4 Illustrative example and results

The numerical results acquired by the LDG technique for the nonlinear KPP (1) are outlined in this section. Here, the entire space domain is split into uniform meshes for spatial discretization. The L_2 and L_∞ error norms

have been obtained in this work to validate the accuracy of the implemented numerical scheme. The error norms are defined on the spatial domain as follows:

$$L_2 = \|u_{\text{exact}} - u_{\text{appx}}\|_2 = \left(\sum_{i=1}^{\mathcal{M}} (u_{\text{exact}}(x_i, T) - u_{\text{appx}}(x_i, T))^2 \right)^{\frac{1}{2}},$$

$$L_\infty = \|u_{\text{exact}} - u_{\text{appx}}\|_\infty = \max_{1 \le i \le \mathcal{M}} |u_{\text{exact}}(x_i, T) - u_{\text{appx}}(x_i, T)|.$$

It is demonstrated that the numerical approximations obtained by the LDG method correspond to the exact traveling wave solutions, and the current LDG method studied in this scientific investigation exhibits robust numerical capabilities in solving an array of NLEEs emerging in various physical, chemical, and biological models.

Example 1. In this example, consider the traveling wave solution (11) obtained by the Kudryashov method for the nonlinear KPP (1) with boundary conditions on $[-5, 5] \times [0, 1]$ given by

$$
\begin{cases}
u(-5, t) = \dfrac{1}{2\delta} \left(-\nu + \sqrt{\nu^2 - 4\delta\mu} \tanh \left(\dfrac{(-5\sqrt{2\delta} - t\nu)\sqrt{\nu^2 - 4\delta\mu}}{4\delta} \right) \right), \\
u(5, t) = \dfrac{1}{2\delta} \left(-\nu + \sqrt{\nu^2 - 4\delta\mu} \tanh \left(\dfrac{(5\sqrt{2\delta} - t\nu)\sqrt{\nu^2 - 4\delta\mu}}{4\delta} \right) \right).
\end{cases}
$$
(27)

The exact traveling wave solution is given by

$$u(x, t) = \frac{1}{2\delta} \left(-\nu + \sqrt{\nu^2 - 4\delta\mu} \tanh \left(\frac{(\sqrt{2}x\sqrt{\delta} - t\nu)\sqrt{\nu^2 - 4\delta\mu}}{4\delta} \right) \right).$$

In this example, the exact solution (11) of KPP (1) is considered with the parameters $\nu = 0.01$, $\mu = -3.1 \times 10^{-4}$, and $\delta = 2.7$ to demonstrate the numerical capabilities of the implemented LDG scheme. The simulation results are obtained by uniformly splitting the computational space domain $[-5, 5]$ into $\mathcal{M} = 5$, $\mathcal{M} = 10$, and $\mathcal{M} = 20$ cells using both piecewise quadratic $(\mathcal{P}^2)$ and cubic $(\mathcal{P}^3)$ elements with time step $\Delta t = 1 \times 10^{-3}$ for various values of t. Tables 1, 2, and 3 display the satisfactory and reasonably minimal L_2

and L_∞ errors at time $t = 0.8$, 0.9, and 1. The data obtained from Tables 1, 2, and 3 clearly demonstrate that the error norms L_2 and L_∞ drop as the mesh is refined. That is, as the values of $\mathcal{M}$ increase. Figure 1 depicts the two-dimensional graphical representation of exact and LDG solutions of KPP (1) for both $\mathcal{P}^2$ and $\mathcal{P}^3$ elements and $\mathcal{M} = 10$ cells at time $t = 0.5$. Figure 2 illustrates the three-dimensional absolute error plot for $u_h(x,t)$ with $\mathcal{P}^3$ element and $\mathcal{M} = 5$ cells, whereas Figures 3 and 4 display the three-dimensional exact and LDG surface solutions using $\mathcal{P}^2$ and $\mathcal{P}^3$ elements, respectively, for $\mathcal{M} = 5$ cells.

Table 1: L_2 and L_∞ errors with CPU time in seconds for KPP (1) at $t = 0.8$.

| Solution	$\mathcal{M}$	$L_2(u)$	$L_\infty(u)$	CPU time
	5	1.0470686E-5	1.0466120E-5	2.749
$\mathcal{P}^2$ element	10	1.0296273E-5	9.7705299E-6	3.906
	20	8.0518960E-6	6.3148590E-6	7.296
	5	6.5980033E-6	6.5921875E-6	4.593
$\mathcal{P}^3$ element	10	6.1202357E-6	5.7864110E-6	13.703
	20	4.7371412E-6	3.6829625E-6	19.421

Table 2: L_2 and L_∞ errors with CPU time in seconds for KPP (1) at $t = 0.9$.

Solution	$\mathcal{M}$	$L_2(u)$	$L_\infty(u)$	CPU time
	5	1.1330156E-5	1.1320364E-5	2.749
$\mathcal{P}^2$ element	10	1.0697374E-5	1.0039300E-5	3.906
	20	8.2778473E-6	6.3542206E-6	7.296
	5	7.0633547E-6	7.0533354E-6	4.593
$\mathcal{P}^3$ element	10	6.3281813E-6	5.9154481E-6	13.703
	20	4.8423464E-6	3.6823185E-6	19.421

Table 3: L_2 and L_∞ errors with CPU time in seconds for KPP (1) at $t = 1$.

Solution	$\mathcal{M}$	$L_2(u)$	$L_\infty(u)$	CPU time
	5	1.2091493E-5	1.2073014E-5	2.749
$\mathcal{P}^2$ element	10	1.1055419E-5	1.0263072E-5	3.906
	20	8.4779126E-6	6.3798095E-6	7.296
	5	7.4723516E-6	7.4558341E-6	4.593
$\mathcal{P}^3$ element	10	6.5113575E-6	6.0190537E-6	13.703
	20	4.9320475E-6	3.6738220E-6	19.421
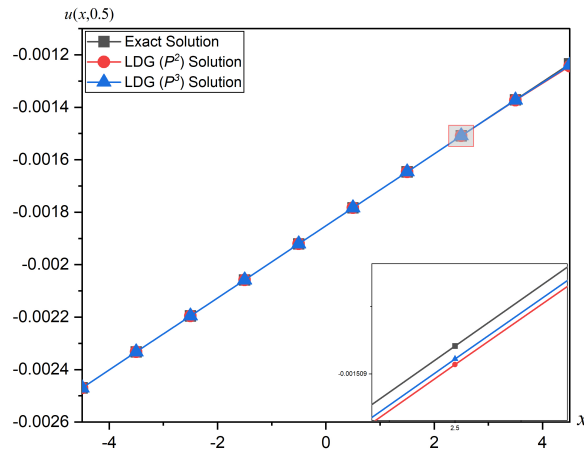
Figure 1: Exact and numerical results of KPP (1) for both $\mathcal{P}^2$ and $\mathcal{P}^3$ elements at $t = 0.5$.
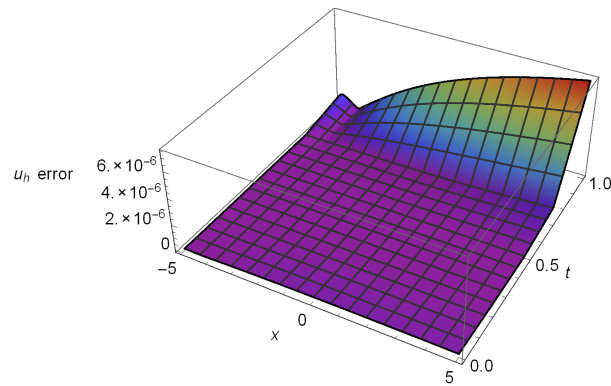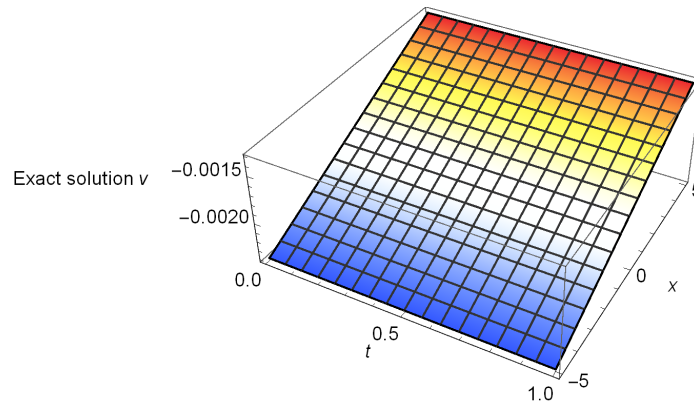
Figure 2: The 3-D absolute error plot of KPP (1) with $\mathcal{P}^3$ element.
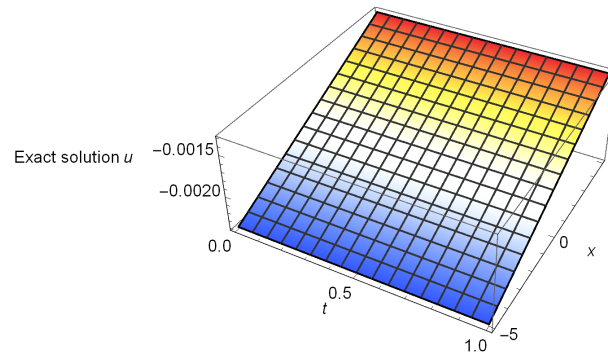
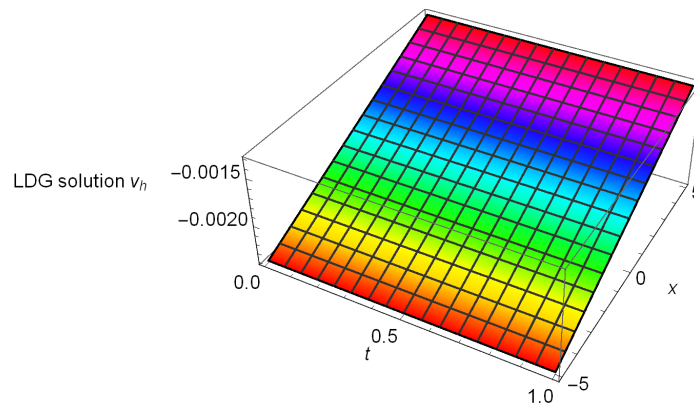
(a) Exact surface solution
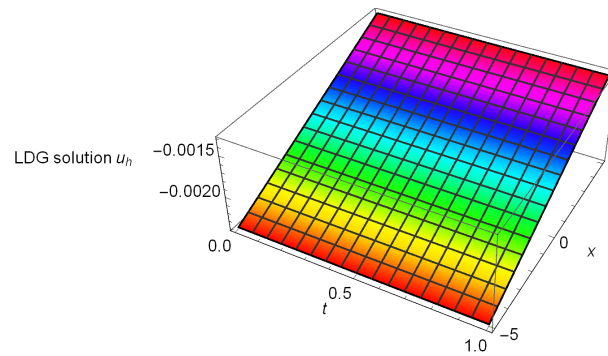
(b) LDG surface solution

Figure 3: Exact and LDG surface solutions of KPP (1) with $\mathcal{P}^2$ element.

(a) Exact surface solution

(b) LDG surface solution

Figure 4: Exact and LDG surface solutions of KPP (1) with $\mathcal{P}^3$ element.

5 Concluding remarks

This work detailed the numerical simulation of the nonlinear KPP (1) using the LDG method. The numerical model framework utilized a third-order TVD-RK discretization technique for the time derivative and a DG finite element discretization technique for the space derivative to generate acceptable numerical solutions. This work also employed the Kudryashov technique to develop exact traveling wave solutions of the governing KPP equation that include the hyperbolic and exponential functions, all with arbitrary parameters. The numerical solutions produced using the LDG scheme demonstrate highly accurate results when compared to the solution obtained using the Kudryashov method. Also, the LDG method for KPP (1) was proved to be L_2 stable by carefully choosing interface numerical fluxes. The selection of these numerical fluxes played a crucial role in ensuring the L_2 stability for the implemented LDG scheme. The numerical data, comprising L_2 and L_∞ errors, demonstrated the efficacy and feasibility of the LDG method algorithm in solving the governing nonlinear KPP (1) and other related NLEEs.

Author contributions

Both authors made equal contributions to the development of the manuscript.

Data availability statement

All the data generated for this study are included in this article.

Funding

Declarations

Ethical approval

Not applicable

Disclosure statement

The author(s) declare(s) that there are no competing interests regarding the publication of this manuscript.

References

[1] Akkilic, A.N., Sulaiman, T.A., Shakir, A.P., Ismael, H.F., Bulut, H., Shah, N.A., and Ali, M.R. *Jaulent–Miodek evolution equation: Analytical methods and various solutions*, Result. Phys. 47 (2023), 106351.

[2] Athanasakis, I., Papadopoulou, E., and Saridakis, Y. *Hermite Collocation and SSPRK Schemes for the Numerical Treatment of a Generalized Kolmogorov–Petrovskii–Piskunov Equation*, In Proceedings of The World Congress on Engineering, 2015.

[3] Carillo, S., and Ragnisco, O. *Nonlinear evolution equations and dynamical systems*, Springer Berlin, Heidelberg, 2012.

[4] Chand, A., and SahaRay, S. *A numerical treatment of the Rosenau–Hyman equation for modeling pattern formation in liquid droplets*, Modern Phys, Lett, B 38 (12) (2023), 2450038.

[5] Chand, A., and SahaRay, S. *Numerical simulation of Allen–Cahn equation with nonperiodic boundary conditions by the local discontinuous Galerkin method*, Int. J. Modern Phys. B 37 (02) (2023), 2350019.

[6] Dehghan, M., and Abbaszadeh, M. *Variational multiscale element free Galerkin (VMEFG) and local discontinuous Galerkin (LDG) methods*

for solving two-dimensional Brusselator reaction–diffusion system with and without cross-diffusion, Comput. Method. Appl. Mech. Engin. 300 (2016), 770–797.

[7] Du, Q., Ju, L., and Lu, J. *A discontinuous Galerkin method for one-dimensional time-dependent nonlocal diffusion problems*, Math. Comput. 88 (315) (2019), 123–147.

[8] Feng, J., Li, W., and Wan, Q. *Using (G'/G)-expansion method to seek the traveling wave solution of Kolmogorov–Petrovskii–Piskunov equation*, Appl. Math. Comput. 217 (12) (2011), 5860–5865.

[9] Ghosh, B., and Mohapatra, J. *A novel numerical technique for solving time fractional nonlinear diffusion equations involving weak singularities*, Math. Method. Appl. Sci. 46 (12) (2023), 12811–12825.

[10] Gottlieb, S., and Shu, C.W. *Total variation diminishing Runge–Kutta schemes*, Math. Comput. 67, 221 (1998), 73–85.

[11] Huang, C., An, N., and Yu, X. *A local discontinuous Galerkin method for time-fractional diffusion equation with discontinuous coefficient*, Appl. Numer. Math. 151 (2020), 367–379.

[12] Inan, B., Osman, M.S., Ak, T., and Baleanu, D. *Analytical and numerical solutions of mathematical biology models: The Newell-Whitehead-Segel and Allen-Cahn equations*, Math. Method. Appl. Sci. 43 (5) (2020), 2588–2600.

[13] Jiao, Y., Wang, T., Shi, X., and Liu, W. *Mixed Jacobi-Fourier spectral method for Fisher equation*, Math. Model. Anal. 23 (2) (2018), 240–261.

[14] Khater, M.M., Attia, R.A., and Lu, D. *Computational and numerical simulations for the nonlinear fractional Kolmogorov–Petrovskii–Piskunov (FKPP) equation*, Physica Scripta 95 (5) (2020), 055213.

[15] Kudryashov, N.A. One method for finding exact solutions of nonlinear differential equations, Commun. Nonlinear Sci. Numer. Simul. 17 (6) (2012), 2248–2253.

[16] Kudryashov, N.A., and Loguinova, N.B. *Extended simplest equation method for nonlinear differential equations*, Appl. Math. Comput. 205 (1) (2008), 396–402.

[17] Li, B.Q. *Discontinuous finite elements in fluid dynamics and heat transfer*, Springer, London, 2006.

[18] Ling, D., Shu, C.W., and Yan, W. *Local discontinuous Galerkin methods for diffusive–viscous wave equations,* J. Comput. Appl. Math. 419 (2023), 114690.

[19] Ma, W.X., and Fuchssteiner, B. Explicit and exact solutions to a Kolmogorov–Petrovskii–Piskunov equation, Int. J. Non-linear Mech. 31(3) (1996), 329–338.

[20] Namjoo, M., and Zibaei, S. *Numerical solutions of FitzHugh–Nagumo equation by exact finite-difference and NSFD schemes*, Comput. Appl. Math. 37 (2018), 1395–1411.

[21] Santra, S., and Mohapatra, J. *Numerical treatment of multi-term time fractional nonlinear KdV equations with weakly singular solutions*, Int. J. Model. Simul. 43 (1) (2023), 23–33.

[22] Tao, Q., Xu, Y., and Shu, C.W. *An ultraweak-local discontinuous Galerkin method for PDEs with high order spatial derivatives,* Math. Comput. 89 (326) (2020), 2753–2783.

[23] Xu, Y., and Shu, C.W. *Local discontinuous Galerkin methods for high-order time-dependent partial differential equations*, Commun. Comput. Phys. 7 (1) (2010), 1.

[24] Yan, J., and Shu, C.W. *Local discontinuous Galerkin methods for partial differential equations with higher order derivatives*, J. Sci. Comput.17 (2002), 27–47.

[25] Yan, Z., and Zhang, H. *New explicit solitary wave solutions and periodic wave solutions for Whitham-Broer-Kaup equation in shallow water*, Phys. Let. A 285, (5-6) (2001), 355–362.